THE JOURNAL OF PHYSICAL CHEMISTRY A

ARTICLE

pubs.acs.org/JPCA

Direct Measurements of the Rate Constants of the Reactions NCN + NO and NCN + NO_2 Behind Shock Waves

J. Dammeier and G. Friedrichs*

Institut für Physikalische Chemie, Christian-Albrechts-Universität zu Kiel, Olshausenstrasse 40, D-24098 Kiel, Germany

Supporting Information

ABSTRACT: The high-temperature rate constants of the reactions NCN + NO and NCN + NO_2 have been directly measured behind shock waves under pseudo-first-order conditions. NCN has been generated by the pyrolysis of cyanogen azide (NCN_3) and quantitatively detected by sensitive difference amplification laser absorption spectroscopy at a wavelength of 329.1302 nm. The NCN_3 decomposition initially yields electronically excited ^{1}NCN radicals, which are subsequently transformed to the triplet ground state by collision-induced intersystem crossing (CIISC). CIISC efficiencies were found to increase in the order of Ar < NO_2 < NO as the collision gases. The rate constants of the NCN + NO/NO_2 reactions can be expressed as $k_{NCN+NO}/(cm^3\ mol^{-1}s^{-1}) = 1.9 \times 10^{12} \exp[-26.3\ (kJ/mol)/RT]$ ($\pm 7\%, \Delta E_a = \pm 1.6$ kJ/mol, 764 K < T < 1944 K) and $k_{NCN+NO_2}/(cm^3\ mol^{-1}s^{-1}) = 4.7 \times 10^{12} \exp[-38.0(kJ/mol)/RT]$ ($\pm 19\%, \Delta E_a = \pm 3.8$ kJ/mol, 704 K < T < 1659 K). In striking contrast to reported low-temperature measurements, which are dominated by recombination processes, both reaction rates show a positive temperature dependence and are independent of the total density (1.7×10^{-6} mol/cm^3 < ρ < 7.6×10^{-6} mol/cm^3). For both reactions, the minima of the total rate constants occur at temperatures below 700 K, showing that, at combustion-relevant temperatures, the overall reactions are dominated by direct or indirect abstraction pathways according to NCN + NO → CN + N_2O and NCN + NO_2 → NCNO + NO.

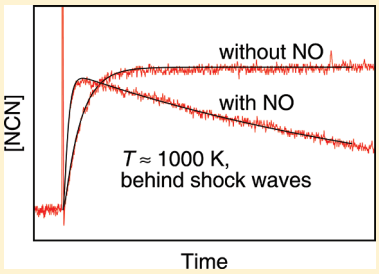

I. INTRODUCTION

Encouraged by the demand for clean energy sources, the efforts to reduce the emissions of hazardous substances from combustion processes continue. Nitrogen oxides NO_x (NO and NO_2) are among the main pollutants, which are generated in the combustion of fossil fuels as well as fuels made from regrowing resources.[1] The hazardous potential of NO_x lies in its contribution to photochemical smog in the troposphere and to ozone depletion in the stratosphere.[2] Furthermore, nitrous oxide (N_2O), a secondary product of NO_x reactions, is an active atmospheric trace gas with a high global warming potential.[3]

There are several formation mechanisms and two principal sources of NO_x in combustion processes.[1] First, NO_x stems from nitrogen impurities in the fuel, which are oxidized. This mechanism is referred to as fuel-N-conversion.[4] Second, NO_x can be generated from atmospheric molecular nitrogen. At high temperatures, the primary formation pathway takes place according to the Zeldovich mechanism:[5,6]

$$O + N_2 \rightarrow NO + N \tag{1}$$

$$N + O_2 \rightarrow NO + O \tag{2}$$

$$N + OH \rightarrow NO + H \tag{3}$$

Third, in low temperature combustion at high pressures, NO_x is yielded via the reaction sequence[7,8]

$$N_2 + O + M \rightarrow N_2O + M \tag{4}$$

$$N_2O + O \rightarrow NO + NO \tag{5}$$

Finally, especially under fuel-rich combustion conditions, prompt-NO is generated by the reaction of small hydrocarbon radicals with N_2. Fenimore[9] suggested that a key initiating step of the reaction sequence is the spin-forbidden reaction

$$CH(^2\Pi) + N_2(^1\Sigma^+) \rightarrow N(^4S) + HCN(^1\Sigma^+) \tag{6a}$$

In fact, it has long been recognized that the intersystem crossing probability from the doublet to the quartet potential energy surface necessary for reaction 6a is low, and thus theoretically predicted rate constants were lower than experimentally measured.[10] In the year 2000, the products of this textbook reaction have been revised by Moskaleva et al.[11,12] according to

$$CH(^2\Pi) + N_2(^1\Sigma^+) \rightarrow H(^2S) + NCN(^3\Sigma_g^-) \tag{6b}$$

By quantum chemical and statistical rate calculations they showed that this spin-allowed reaction constitutes a relevant pathway and yields rate constants that are consistent with the experimental data. The pathway generates NCN radicals, a species which had not been discussed in the context of combustion research before. Later, it was experimentally proven by flame and shock tube measurements that the NCN channel (reaction 6b) is in fact the dominating reaction channel of reaction 6.[13−16] Since then, several

Received: September 9, 2011
Revised: November 5, 2011
Published: November 08, 2011

theoretical[11,17−19,21−23] and experimental[16−18,24−27] studies have addressed NCN reactions and available rate constants have been introduced into existing combustion models.[14,27−31]

Objects of previous theoretical work were the reactions NCN + O (7),[22] NCN + O_2 (8),[21] NCN + OH (9),[23] NCN + NO (10),[17,19,20] NCN + NO_2 (11),[18] and NCN + H (12).[11] Rate constants and product branching ratios have been theoretically predicted over a wide range of temperatures and pressures. In contrast, available experimental results are limited to a few reactions and mainly to temperatures below T < 600 K. An exception is the reaction NCN + H, which has been investigated behind shock waves in the temperature range 2378 K < T < 2492 K by Vasudevan et al.[16] NCN was obtained by the pyrolysis of ethane (C_2H_6), which yields CH radicals that subsequently reacted with the bath gas N_2 to form NCN (reaction 6b). Observed NCN decays were attributed to the reaction NCN + H (12). An indirect determination of the rate constant of reaction 12 has also been reported by Lamoureux et al.[27] In a combined modeling and flame diagnostics study, they attributed deviations of the simulated from the measured CH, NCN and NO concentrations to reaction 12. Furthermore, high-temperature reaction rates of the unimolecular NCN decomposition NCN + M → C + N_2 + M (13) have been directly measured (C-ARAS) behind shock waves at temperatures of 1800−2950 K.[32,33]

Recently, in order to provide much needed high temperature rate constant data for bimolecular NCN reactions, we have thoroughly investigated the thermal decomposition of NCN_3 as a quantitative high-temperature NCN radical source.[34] NCN formation rates and high temperature absorption cross section have been directly measured showing that NCN can be sensitively detected in the parts per million (ppm) range behind shock waves. At such low concentrations, subsequent NCN secondary chemistry is efficiently suppressed turning the thermal NCN_3 decomposition into an ideal NCN radical source. Nevertheless, as a requirement for accurate rate constant measurements, a consistent NCN background mechanism has been derived from pyrolysis experiments reporting rate constants for the reactions NCN + M (13) at 2010 K < T < 3250 K and NCN + NCN (14) at 965 K < T < 1900 K.[35] Furthermore, by adding O atoms generated from the N_2O decomposition to the reaction mixtures, we were able to measure the rate constant of the reaction NCN + O (7) for the first time (1825 K < T < 2785 K).

Regarding reaction 10, NCN + NO, the theoretical investigations agree that the reaction proceeds via an NCNNO intermediate.[17,19,20,25] Huang et al.[17] performed quantum chemical (G2M/CC5) and statistical rate (VTST/RRKM/ME) calculations. It was found that the overall reaction exhibits negative temperature dependence at T < 500 K and a pronounced positive temperature dependence toward higher temperatures. At low temperatures, a recombination reaction according to NCN + NO + M ⇌ NCNNO + M takes place, whereas at high temperatures an indirect abstraction channel yields N_2O + CN. One of the first experimental works on elementary NCN gas phase reactions was concerned with reaction 10 and was performed by Baren and Hershberger[24] in 2002. NCN was generated by 193 nm photolysis of diazomethane (CH_2N_2) in the presence of cyanogen (C_2N_2). Rate constants could be determined from NCN concentration−time profiles measured by means of laser-induced fluorescence (LIF) in the temperature range 298 K < T < 573 K. Both NCN (by LIF) and the possible products N_2O and CO_2 (by IR absorption) were detected. Similarly, Huang et al.[17] measured rate constants in the temperature range of 254 K < T < 353 K following the 193 nm photolysis of cyanogen azide (NCN_3) as a source of NCN. In the examined temperature range, both studies support the expected negative temperature dependence. Welz[25] extended the temperature range to 254 K < T < 485 K and characterized the pressure dependence at pressures ranging from p = 30 mbar to p = 50 bar. Again, NCN was detected by LIF following the photodissociation of NCN_3 at λ = 193 nm and λ = 248 nm.

Reaction 11, NCN + NO_2, has been the subject of two combined experimental and theoretical studies. Yang et al.[18] measured rate constants in the temperature range 260 K < T < 296 K at pressures between p = 133 mbar and p = 666 mbar. NCN was generated by 193 nm photolysis of NCN_3 and detected by LIF. Additionally, rate constants have been calculated at temperatures of 200 K < T < 2000 K using a combination of quantum mechanical (G2M//B3LYP/6-311+G(d)) and statistical (RRKM/ME) methods. On the basis of these calculations, an association reaction is expected for temperatures T < 700 K to take place exhibiting a negative temperature dependence, whereas at higher temperatures a positively temperature-dependent abstraction channel is predicted to yield NCNO + NO. In similar experiments, Kappler[26] extended the temperature range to 255 K < T < 349 K and measured falloff curves in the pressure range 155 mbar < p < 38 bar. In agreement with Yang et al., a negative temperature and a positive pressure dependence has been noted, which was explained by an association−isomerization mechanism finally yielding NCO and N_2O as the products.

So far, only the low-temperature recombination processes of reactions 10 and 11 could be experimentally confirmed. High-temperature experiments suitable to assess the dominating N_2O + CN channel for reaction 10 and NCNO + NO for reaction 11 are not available. In this spirit, the high-temperature measurements presented in this paper provide an opportunity to bring together theory and experiment. Assessing and characterizing the temperature and pressure dependencies of bimolecular reactions of small radicals, i.e., the preference of an association complex at low temperatures and the opening of an activation energy-controlled direct or indirect abstraction reaction channel at high temperatures, remains challenging. Recent examples from our shock tube lab addressing similar problems are the measurements of the rate constants of the reactions HCO + NO/NO_2[36] and HCO + O_2.[37]

In this paper, first high-temperature measurements on the reactions

$$\mathrm{NCN} + \mathrm{NO} \rightarrow \mathrm{N_2O} + \mathrm{CN} \tag{10}$$

and

$$\mathrm{NCN} + \mathrm{NO_2} \rightarrow \mathrm{NCNO} + \mathrm{NO} \tag{11}$$

will be presented to provide rate constant data at combustion relevant temperatures and to verify the theoretically predicted dominance of the direct or indirect abstraction reaction channels.

II. EXPERIMENTAL SECTION

All experiments have been performed using a shock tube setup[37,38] equipped with a narrow bandwidth laser absorption spectrometer[34] to measure NCN concentration−time profiles. Briefly, the 4.4 m long test section of the shock tube with an inner diameter of 81 mm could be evacuated down to pressures of 10^{-7} mbar by a combination of oil-free diaphragm and turbomolecular

Table 1. Selected Reactions of the Mechanism Used in the Numerical Simulations to Extract the Rate Constants of the Reaction NCN + NO[a]

no.	reaction	A	E_a	ref.	
(10)	$^3NCN + NO \rightarrow CN + N_2O$	1.9×10^{12}	26.3	this work	set equal for ^1NCN, see text
(15)	$NCN_3 \rightarrow {}^1NCN + N_2$	3.3×10^9	71.2	44	$\rho = 1.8 \times 10^{-6}$ mol/cm^3
		5.0×10^9	71.2	44	$\rho = 3.5 \times 10^{-6}$ mol/cm^3
(16)	$^1NCN \rightarrow {}^3NCN$	1.1×10^6	17.4	this work	1.0% NO, $\rho = 1.8 \times 10^{-6}$ mol/cm^3
		2.3×10^6	17.4	this work	1.0% NO, $\rho = 3.5 \times 10^{-6}$ mol/cm^3
(19)	$^3NCN + CN \rightleftharpoons C_2N_2 + N$	1.3×10^{14}	33.5	11	
(20)	$^3NCN + N \rightleftharpoons CN + N_2$	1.0×10^{13}		48	

[a] Possible secondary chemistry has been taken into account by the GRI-Mech. 3.0[40] and a subset of NCN and CN reactions as outlined in our previous paper.[35] Rate constants are given as $k_i = AT^n \exp[-E_a/RT]$. Units are cm, mol, s, K and kJ.

Table 2. Selected Reactions of the Mechanism Used in the Numerical Simulations to Extract the Rate Constants of the Reaction NCN + NO$_2$[a]

no.	reaction	A	E_a	ref.	
(7)	$^3NCN + O \rightleftharpoons CN + NO$	9.6×10^{13}	5.8	35	set equal for ^1NCN, see text
(11)	$^3NCN + NO_2 \rightarrow NCNO + NO$	4.7×10^{12}	38.0	this work	set equal for ^1NCN, see text
(15)	$NCN_3 \rightarrow {}^1NCN + N_2$	5.0×10^9	71.2	44	$\rho = 3.5 \times 10^{-6}$ mol/cm^3
		7.7×10^9	71.2	44	$\rho = 7.0 \times 10^{-6}$ mol/cm^3
(16)	$^1NCN \rightarrow {}^3NCN$	2.3×10^6	30.1	this work	0.7% NO_2, $\rho = 3.5 \times 10^{-6}$ mol/cm^3
		1.7×10^6	24.8	this work	0.7% NO_2, $\rho = 7.0 \times 10^{-6}$ mol/cm^3
(17)	$NO_2 + M \rightleftharpoons NO + O + M$	4.0×10^{15}	251	51	
(21)	$NO_2 + NO_2 \rightleftharpoons 2NO + O_2$	2.0×10^{12}	105	51	
(22)	$NO_2 + NO_2 \rightleftharpoons NO_3 + NO$	1.0×10^{13}	108	51	
(23)	$NO_2 + O \rightleftharpoons NO + O_2$	3.9×10^{12}	−1	52	
(24)	$NO_3 + M \rightleftharpoons NO_2 + O + M$	4.0×10^{17}	200	51	
(25)	$NO_3 + O \rightleftharpoons NO_2 + O_2$	1.0×10^{13}		52	

[a] Possible secondary chemistry has been taken into account by the GRI-Mech. 3.0[40] and a subset of NCN and CN reactions as outlined in our previous paper.[35] Rate constants are given in terms of $k = A \exp[-E_a/RT]$. Units are cm, s, mol and kJ.

pump (Pfeiffer Vacuum). Hydrogen, nitrogen or mixtures of hydrogen and nitrogen were used as the driver gases; diaphragms were made from 30 or 80 μm thick aluminum foil. Pressures and temperatures behind shock waves were calculated based on pre-shock conditions, and the shock wave velocity was measured by a fast count unit wired to four piezo-electric sensors (PCB Piezotronics M113A21). Real gas effects and the shock wave damping on the order of 1% were taken into account.

NCN has been detected in its triplet ground state at a wavelength of $\lambda = 329.1302$ cm^{-1} (superposition of the $^3\Pi_1$ sub-band of the $\tilde{A}^3\Pi_u(000) - \tilde{X}^3\Sigma_g(000)$ transition and the Q_1 band head of the $^3\Sigma^+(010) - {}^3\Pi(010)$ vibrationally excited Renner-Teller split transition) by a difference amplification laser absorption scheme. Laser light (1.5 mW) of the respective wavelength was generated by internal frequency doubling of a stabilized continuous wave ring-dye laser (Coherent 899) with DCM Special (Radiant Dyes) as a dye, which was pumped by a Nd:YVO$_4$ solid state laser (Coherent Verdi V10) at $\lambda = 532$ nm. The wavelength of the fundamental has been measured by an interferometric type wavemeter (MetroLux WL200) with an accuracy of ±0.0015 cm^{-1}. Detection and reference beam were divided by a 50:50 beam splitter plate, the detection beam was passed through the shock tube and the reference beam could be attenuated by a variable neutral density filter. Both beams were band-pass filtered and coupled into two optical fibers (Thorlabs BF H22-550), which were connected to a balanced photo detector and amplifier (Thorlabs PDB150A-EC). The resulting difference signal was further amplified (Ortec Fast Preamp 9305) low pass filtered by 1.4 MHz and stored by an analog input board (PCI-DAS4020/12, 20 MHz, 12 bit). The absorption signals were transformed into concentrations using the previously determined NCN absorption cross section ($\log_{10}(\sigma/\text{cm}^2/\text{mol})) = 8.9-8.3 \times 10^{-4} \times T/K$).[34]

The measurements were evaluated by fitting numerical simulations to the measured concentration−time profiles using an appropriate reaction mechanism including reaction rate constants for NCN forming and consuming reactions (see Tables 1 and 2).

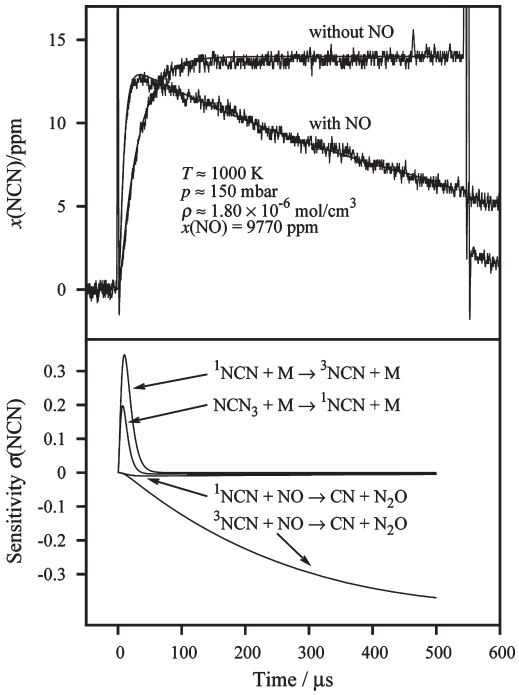

Figure 1. Upper: NCN Concentration−time profiles for experiments with and without NO added to the reaction mixtures. With NO: T = 996 K, p = 149 mbar, $\rho = 1.80 \times 10^{-6}$ mol/cm^3, $x(NCN_3)$ = 13.4 ppm; without NO: T = 1002 K, p = 150 mbar, $\rho = 1.81 \times 10^{-6}$ mol/cm^3, $x(NCN_3)$ = 14.0 ppm. Below: Sensitivity analysis of the experiment with NO.

Numerical simulations were performed using the Chemkin-II[39] program package. For sensitivity analysis, the sensitivity coefficient $\sigma(i,j,t)$ for reaction i of species j at time t was normalized with respect to the maximum concentration c_{max} of the species j over the time history, $\sigma(i,j,t) = 1/c_{max} \times (\partial c(j,t)/\partial \ln k_i)$. The GRI-Mech 3.0 natural flame mechanism[40] has been used as a background mechanism and an additional subset of reactions taking into account NCN and CN secondary chemistry has been adopted from our previous paper.[35] Rate constants of reverse reactions have been taken into account based on thermodynamic data from Konnov,[41] except for NCN, for which the data were taken from Goos et al.[42]

NCN was generated by the thermal decomposition of NCN_3. NCN_3 was synthesized from gaseous BrCN and solid NaN_3 using a variant[34] of the method described by Milligan et al.[43] NCN_3 is an extremely explosive substance, hence, no attempt was made to further purify the initially generated gas. Its purity was checked by means of FTIR spectroscopy. Remaining BrCN impurities were usually <1% and never exceeded 3%. CO_2 was on the order of 0.01% and water was not detectable. Freshly prepared NCN_3 was immediately diluted by argon down to mole fractions of 0.1%, nevertheless, a slow decomposition of ∼5% per day was found to take place.

Gases and chemicals used were argon (Air Liquide, 99.99%), hydrogen and nitrogen as driver gases (Air Liquide, 99%), NO and NO_2 (Air Liquide, 99.95%), BrCN (Acros, 97%), and NaN_3 (Merck, 99%). Gas mixtures were prepared using the partial pressure method; the NO_2/N_2O_4 equilibrium has been taken into account. NO and NO_2 were purified by repeated freeze−pump−thaw cycles. All gas mixtures were used within 3 days after preparation. Before all shock tube experiments, the shock tube was flushed with the respective test gas mixtures at a pressure of $p \approx 50$ mbar. No dependence of measured signals on the flushing time or the time between sample preparation and experiment could be noticed revealing that wall absorption effects or room temperature reactions of NCN_3 with NO or NO_2 did not perturb the measurements.

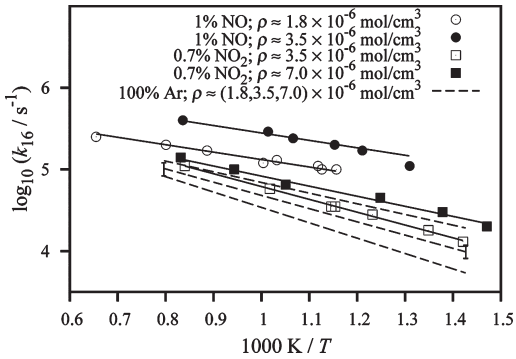

Figure 2. Arrhenius plot of measured first order CIISC rate constants at several total densities with NO or NO_2 added to the gas mixtures. Arrhenius expressions of rate constants in pure Ar have been determined from ^{1}NCN concentration−time profiles[44] and are shown as dashed lines.

III. RESULTS AND DISCUSSION

A. NCN + NO. NCN concentration−time profiles of mixtures of NCN_3 and NO behind incident shock waves have been recorded in the temperature range 764 K < T < 1944 K at two different total densities of $\rho \approx 1.8 \times 10^{-6}$ mol/cm^3 and $\rho \approx 3.5 \times 10^{-6}$ mol/cm^3 (123 mbar < p < 690 mbar). Mole fractions of NCN_3 were between 5 and 15 ppm and much lower than the mole fractions of the excess component NO, which were 5000 or 10000 ppm. A typical concentration−time profile together with the respective numerical simulation and a sensitivity analysis is shown in Figure 1. To illustrate the influence of added NO, an experiment without NO is shown as well. Two strong Schlieren signals accompany the incident and reflected shock wave passages and thus define t = 0 of the corresponding temperature and pressure jumps.

Without the addition of NO, NCN consuming reactions are negligible. Up to temperatures of T = 2000 K, stable NCN plateaus were found. At higher temperatures, the decomposition of NCN set in according to NCN + M → C + N_2 (13). The initial increase of the NCN absorption signal in Figure 1 reflects two processes: The decomposition of the precursor molecule NCN_3 yielding ^{1}NCN and the subsequent relaxation of the electronically excited ^{1}NCN to its triplet ground state (^{3}NCN) via collision-induced intersystem crossing (CIISC):

$$NCN_3(+M) \rightarrow {}^1NCN + N_2(+M) \quad (15)$$

$$^1NCN(+M) \rightarrow {}^3NCN(+M) \quad (16)$$

Rate constants for both processes have been reported in our previous publications.[34] Updated rate constant expressions as used in this work rely on recent ^{1}NCN concentration−time profile measurements, which will be reported elsewhere.[44] Upon the addition of 0.5 − 1% NO, the initial increase of the ^{3}NCN signal gets much faster. Since the unimolecular decomposition process can be expected to be only slightly affected by such small amounts of a

different bath gas, this increase is attributed to a much more efficient CIISC process of NO compared to argon. To support this assumption, test experiments have been performed with the detection laser frequency tuned to a strong ^{1}NCN transition ($\tilde{\nu}$ = 30045.46 cm^{-1}). In the measured ^{1}NCN concentration−time profiles, the addition of NO did not alter the formation rate of ^{1}NCN, but had a strong influence on the ^{1}NCN decays.

With 1% NO added to the mixture, rise times are shortened by a factor of about 5 showing that NO exhibits a CIISC efficiency higher by a factor of 400 compared to argon. Such a strong dependence of the CIISC efficiency on the nature and spin state of the collision gas is not unusual. For example, in the case of ^{1}NH, collisions with Xe lead to CIISC rate constants 3 orders of magnitude higher than collisions with Ar.[45] Rate constants of the relaxation reaction 16 were extracted from the measured profiles and are shown together with corresponding data for argon[44] and NO_2 (see Section III.B) in Figure 2. Similar values of the apparent activation energies on the order of 20 kJ/mol are found for NO, NO_2 and Ar. The apparent activation energies as well as the observed density dependences ($n \approx 1$ for NO, $n \approx 0.5$ for NO_2, $n \approx 0.6$ for Ar; according to $k_b = ((\rho_b)/(\rho_a))^n k_a$) reflect the complicated underlying physical processes that govern the CIISC probability and are difficult to predict.[46,47]

As it is discernible in the sensitivity analysis shown in the lower frame of Figure 1, the CIISC process is completed within 50 μs and thus does not critically interfere with the rate constant measurement of the reaction NCN + NO. In fact, reaction 10 is the only sensitive NCN consuming reaction showing that the measurements essentially follow pseudo-first-order kinetics. Possible secondary chemistry is successfully suppressed by using very low (∼10 ppm) mole fractions of NCN_3. Rate constants were extracted in the temperature range of 764 K < T 1944 K. Toward low temperatures, the accessible temperature range was limited by the rate of the NCN_3 decomposition. It is slower than the ^{1}NCN relaxation below T = 750 K. At high temperatures, NCN absorption cross sections are too low, and higher NCN_3 concentrations used to compensate for the lower sensitivity resulted in significant secondary chemistry. Selected rate constants of the reaction used in the mechanism can be found in Table 1.

An Arrhenius plot of the rate constant data for k_{10} including selected literature results[17,24,25] is shown in Figure 3. Data of the experimental conditions are given in the Supporting Information. No dependence of the measured rate constants on the total density is discernible within the scatter of the data. All data points fall within a narrow margin and can be very well represented by the Arrhenius expression:

$$k_{10}/(\mathrm{cm^3mol^{-1}s^{-1}}) = 1.89 \times 10^{12} \exp[-26.3(\mathrm{kJ/mol})/RT](\pm 7\%)$$

The stated error estimate reflects a combination of the statistical error of the Arrhenius fit (±1%, 2σ), uncertainties of the NO mole fraction (±5%), and uncertainties in the ^{3}NCN formation mechanism (±1%). Due to the pseudo-first-order reaction conditions, uncertainties of the NCN absorption cross section and thus NCN concentration did not result in an additional error. The uncertainty of the Arrhenius activation energy of ±1.6 kJ/mol corresponds to the 2σ error of the slope of the Arrhenius fit.

In additional measurements, ^{1}NCN concentration−time profiles have been recorded at a detection wavelength of λ = 332.8290 nm to assess potential differences of the reactivities of ^{1}NCN and ^{3}NCN. Unfortunately, because of the fast CIISC process, the evaluation of these signals did not yield reliable rate constants for

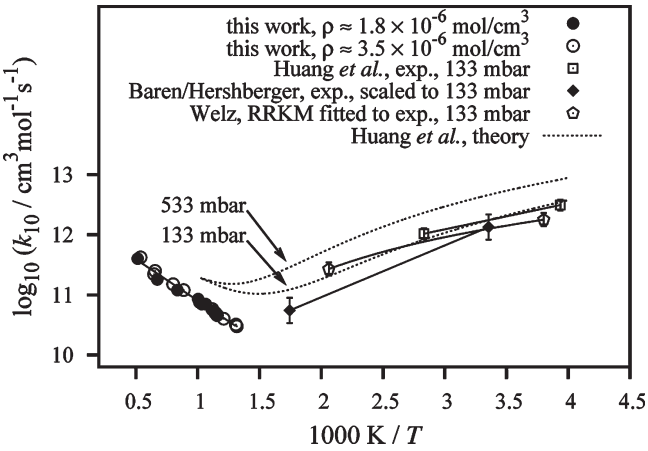

Figure 3. Comparison of measured rate constants of reaction 10, NCN + NO, with selected literature data.[17,24,25] The literature values of Baren and Hershberger[24] and Welz[25] have been scaled to 133 mbar based on the Troe parameters given in the work of Welz.

the reaction ^{1}NCN + NO. However, as the observed absolute ^{3}NCN mole fractions were found to be in quantitative agreement with the initial NCN_3 precursor mole fractions within error limits, a major influence of the reaction ^{1}NCN + NO can be ruled out anyway. Given that no literature data are available, for the sake of a complete reaction mechanism, the ^{1}NCN and ^{3}NCN radical reactions have been assumed to proceed with the same rate. From detailed simulations of the absolute ^{3}NCN yield, at least an upper limit for the ^{1}NCN reaction could be estimated. According to these simulations, a factor of 20 higher reaction rate constant for ^{1}NCN + NO should have caused a detectable decrease of ^{3}NCN yield. On one hand, using such a high value in the numerical simulations would have resulted in a merely 20% smaller rate constants for the CIISC process, but would not have altered our general conclusion that NO is a much more efficient collider than Ar. On the other hand, the same rate constants would have been obtained for the reaction ^{3}NCN + NO. These were extracted from the pseudo-first-order decays of the ^{3}NCN profiles at long reaction times, whereas any influence of ^{1}NCN is restricted to the first few microseconds.

In contrast to all previous experimental studies, which have been performed at temperatures below T = 573 K, a positive temperature dependence has been found at temperatures greater than 764 K. This positive temperature dependence has been predicted by Huang et al.[17] in their theoretical study. In Figure 3, theoretically derived rate constant expressions for two different total pressures are shown. At low temperatures, according to a recombination process, the reaction proceeds close to the low pressure limit at the investigated pressures p < 1 bar. The corresponding density dependence is also supported by the experimental studies.[17,24,25] In contrast, at high temperatures we find reaction rates that are independent of the total density. Rate constant values are approximately a factor of 2 lower than the Huang et al.[17] prediction. Although no direct evidence of the postulated minimum of the rate constants is provided by our measurements, all experimental data are consistent with a minimum at a temperature around $T \approx 670$ K.

A qualitative explanation of the complex temperature and pressure dependences can be illustrated on the basis of the characteristics of the potential energy surface. A more detailed assessment, however, would have to rely on a full master equation

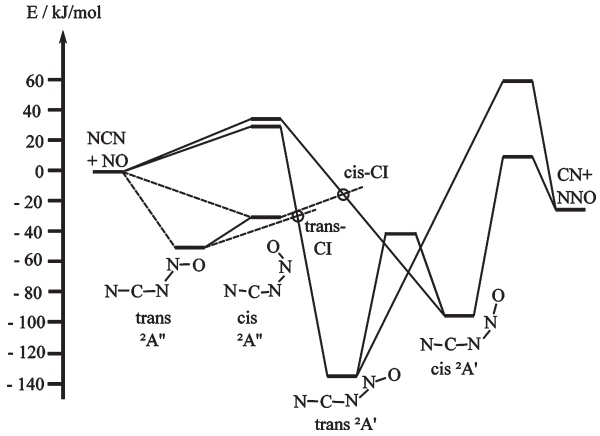

Figure 4. Part of the potential energy surface of the reaction NCN + NO 10 (G2M/CC5//B3LYP/6-311+G(d) level of theory), adopted from Huang et al.[17]

analysis. A simplified scheme of the potential energy surface, adopted from the calculations of Huang et al.,[17] is outlined in Figure 4. Other possible reaction channels forming CNO + N_2 or NCO + N_2 do not play a role because the barriers on the corresponding minimum energy paths are too high. Two different electronic states are involved. A simple association of NCN and NO leads to the $^2A''$state (dashed lines) of NCNNO with two different isomers denoted cis-$^2A''$ and trans-$^2A''$. The reaction continues by crossing to the $^2A'$ surface through two conical intersections (CI) yielding the local minima trans-$^2A'$ and cis-$^2A'$ NCNNO. Further dissociation to the products CN + N_2O involves barriers that are significantly higher in energy than the entrance energy of the initial NCN + NO fragments. At low temperatures, these barriers prevent the formation of the products CN + N_2O. Instead, the *trans*- and *cis*-NCNNO intermediates can be stabilized by collisions. At not too high pressures, the formation of the $^2A'$ isomers dominates.[17] Consequently, the reaction exhibits the typical behavior of a recombination reaction, i.e., a negative temperature dependence (faster redissociation to the reactants at higher temperature) and a positive pressure dependence (collisional stabilization of the intermediates). Toward high temperatures, however, enough thermal energy is involved to overcome the exit barriers of the *cis*- and *trans*-$^2A'$ intermediates. Moreover, due to the increasingly fast forward reaction, collisional stabilization becomes less significant. This is the reason why virtually no pressure dependence has been observed in our experiments. Hence, the forward reaction resembles an indirect abstraction reaction with a positive temperature dependence stemming from the exit barrier. The measured activation energy of E_a = 26 kJ/mol is between the barriers of the *trans*- (61 kJ/mol with respect to the reactants) and the *cis*-$^2A'$ (14 kJ/mol) pathways. The much closer agreement with the cis value reveals that the overall reaction at high temperatures is dominated by the cis pathway.

B. NCN + NO_2. The kinetics of the reaction NCN + NO_2 → NCNO + NO 11 has been investigated in the temperature range 704 K < T < 1659 K and at two different total densities of $\rho \approx 3.5 \times 10^{-6}$ mol/cm^3 and $\rho \approx 7.0 \times 10^{-6}$ mol/cm^3. Corresponding pressures were 182 mbar < p < 654 mbar. Initial mole fractions of NCN_3 in Ar were between 3 and 14 ppm, mole fractions of the excess component NO_2 were 7000 ppm or, for a validation experiment, 19000 ppm. Detailed data of the experimental conditions are given in the Supporting Information. Figure 5 shows a

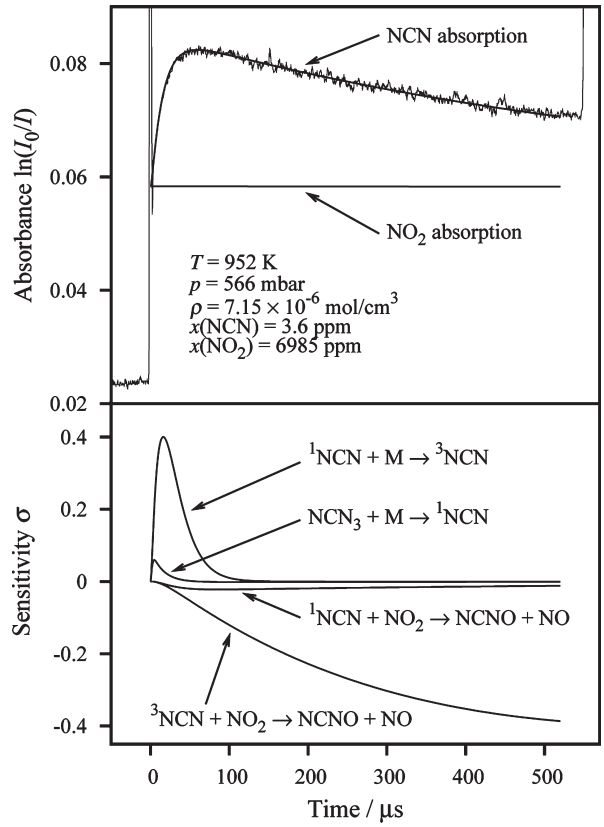

Figure 5. Upper: Absorbance-time profile of an NO_2 experiment behind an incident shock wave. Both NO_2 absorbance and NCN absorbance are shown. Due to the interfering NO_2 background absorption, the baseline is not zero. Lower: NCN sensitivity analysis indicating pseudo-first-order conditions after 100 μs.

typical absorbance-time profile. Absorbance of NCN has been used instead of NCN mole fractions to illustrate the effect of interfering NO_2 background absorption stemming from its broad $\tilde{A}^2B_2$−$\tilde{X}^2A_1$ transition.[49] Already before the arrival of the shock wave, significant NO_2 absorption is discernible. Due to the higher density, higher background absorption values are observed behind the incident shock wave. Superimposed to this background absorption, the NCN absorbance profile indicates the thermal decomposition of NCN_3 followed by CIISC and ^{3}NCN formation. The decay at longer times can be attributed to reaction 11, NCN + NO_2.

In order to take into account NO_2 background absorption, temperature-dependent NO_2 absorption cross sections at $\tilde{\nu}$ = 30383.11 cm^{-1} had been measured beforehand in experiments without NCN_3. NO_2 absorption coefficients are best represented by the expression

$$\log_{10}(\sigma/\mathrm{cm}^2\mathrm{mol}^{-1}) = 5.28 - 1.21 \times 10^{-4} \times T/K$$

An extrapolation to room temperature yields a value of 1.8 × 10^5 cm^2/mol, thus in very good agreement with a value of 1.9 × 10^5 cm^2/mol reported by Bogumil et al.[50] A plot of the measured cross sections can be found in the Supporting Information. NO_2 concentration−time profiles were simulated based on the initial NO_2 concentrations and the reaction mechanism summarized in Table 2. Corresponding absorbance values are denoted "NO_2 absorption" in Figures 5 and 6. Remaining absorbances have been attributed to NCN absorption, which could be extracted from the profiles with high precision. As for the reaction ^{1}NCN + NO, no

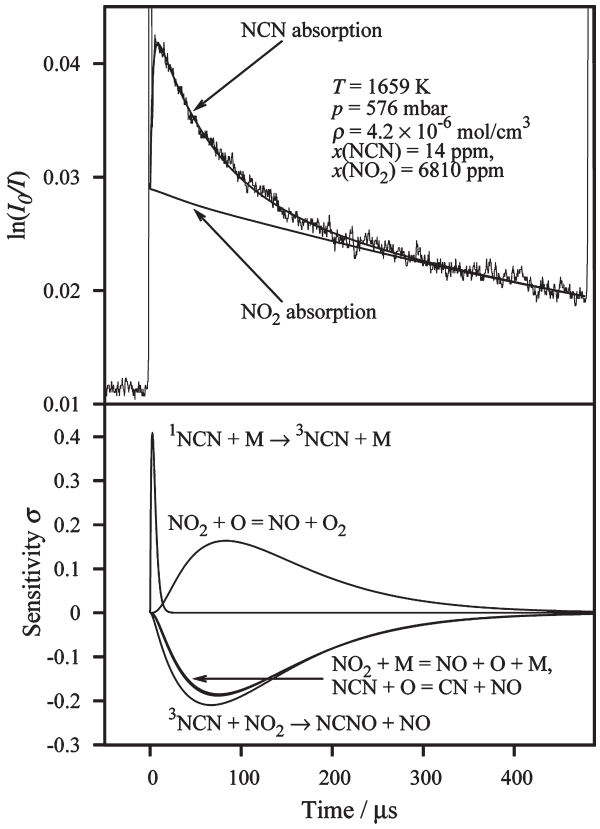

Figure 6. High-temperature NO_2 experiment and corresponding NCN sensitivity analysis.

indication was found for a significant influence of the reaction $^1NCN + NO_2$. Nevertheless, for the sake of a completeness, we included this reaction in the mechanism by assuming the same rate constant for the singlet and triplet reactions.

CIISC rate constants extracted from the resulting NCN concentration−time profiles are included in Figure 2. The relaxation process mediated by collisions with NO_2 is less efficient than with NO, but still a factor of approximately 40 more efficient than with argon. After 100 μs, the ^3NCN formation is completed, and a decay of the absorption can be observed in Figure 5. The sensitivity analysis reveals that reaction 11 is the only important reaction for the consumption of NCN. In this regard, the experimental conditions are close to pseudo-first-order conditions and thus enable an accurate determination of k_{11}. However, at temperatures of >1400 K, more reactions gain importance. Such an experiment is shown in Figure 6. The unimolecular decomposition of NO_2, $NO_2 + M \rightarrow NO + O + M$ (17) sets in, and thus the consecutive reaction NCN + O (7) plays a role. This interfering secondary chemistry constitutes a high temperature limit for k_{11} measurements of about $T \approx 1700$ K. Again, the low temperature limit was set by the decomposition rate of NCN_3.

Measured rate constant values are compared to selected literature data in Figure 7. All data points can be nicely represented by a straight Arrhenius fit, thus supporting the reliability of the applied evaluation procedure.

$$k_{11}/(\mathrm{cm^3mol^{-1}s^{-1}}) = 4.7 \times 10^{12} \exp[-38.0(\mathrm{kJ/mol})/RT](\pm 19\%)$$

At temperatures 704 K < T < 1659 K, the rate constants were found to be independent of the total density. The stated error results from a 5% uncertainty of the NO_2 concentration, a 7% statistical error (2σ), and 2% uncertainty attributable to the precursor molecule decomposition and the singlet cyanonitrene relaxation mechanism. Although uncertainties resulting from possible inaccuracies of the NO_2 decomposition mechanism are only relevant at the high-temperature limit, based on simulations with varied k_{17}, allowance was made for an additional 5% error for k_{11}. The Arrhenius activation energy is accurate to $\Delta E_a = \pm 3.8$ kJ/mol. This estimate already includes the potential uncertainty of the high temperature data points resulting from the NO_2 decomposition mechanism.

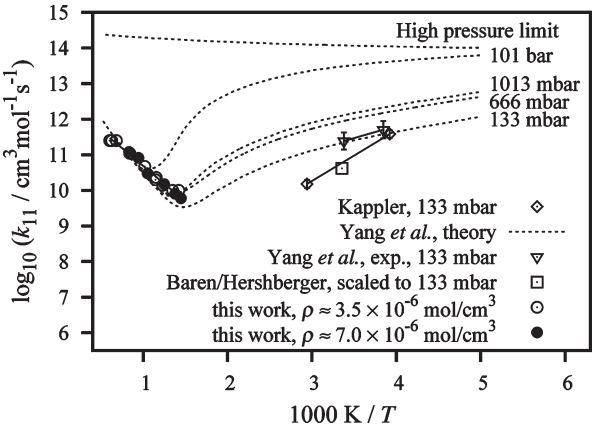

Figure 7. Arrhenius plot of the measured rate constants for the reaction NCN + NO_2 at two different total densities. For comparison, low-temperature experimental data[18,24,26] as well as theoretical predictions of Yang et al.[18] are also shown. The original 4 mbar value of Baren and Hershberger[24] has been scaled to a pressure of 133 mbar based on the Troe parameters reported by Kappler.[26]

Selected results from the literature[18,24,26] are also included in Figure 7. At room temperature, all results are in very good agreement, but toward higher temperatures, differences become apparent. The rate constant data by Kappler[26] exhibit a significantly stronger temperature dependence than those measured by Yang et al.[18] In both studies, rate constants have been determined assuming pseudo-first-order conditions, thus excluding secondary chemistry. However, as Kappler already discussed in her work, the used excimer laser photolysis at λ = 248 nm next to NCN radicals also generates NO and O atoms from NO_2 photolysis, $NO_2 \xrightarrow{h\nu} NO + O$ (18). The possible overestimation of the determined rate constants due to the very fast subsequent reaction 7, NCN + O, was estimated by Kappler to be <5%. Yang et al. used 193 nm instead of 248 nm photolysis. At this wavelength, NO_2 absorption cross sections are much larger, and O atom yields can be expected to be higher. Although Yang et al. argued that O atom formation did not interfere in their experiments due to subtle diffusion effects, the neglected O atom chemistry via reaction 7 may account for the differences and the data of Kappler can therefore be assumed to be more reliable. The dashed curves in Figure 7 represent the theoretical fit of Yang et al. Clearly, a strong pressure dependence emerges. However, due to the mentioned effect, the low temperature rate constants may be somewhat overpredicted.

Our data represent the first high-temperature measurements and can only be compared with the theoretical prediction of Yang et al.[18] In agreement with their work and similar to the reaction NCN + NO, a positive temperature dependence is found at high temperatures. Note that for the temperature and pressure range of this work (182 mbar < p < 654 mbar), the overall reaction is

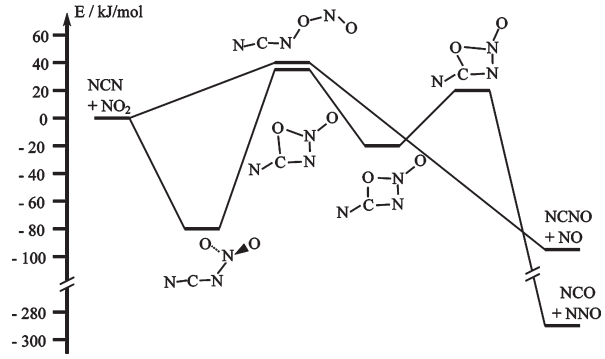

Figure 8. Part of the potential energy surface of the reaction NCN + NO_2 (11) (G2M//B3LYP/6-311+G(d) level of theory), adopted from Yang et al.[18]

predicted to be almost independent of the experimental pressure. The predicted absolute values of k_{11} and the absence of pressure dependence is in very good agreement with our data. Only at the lowest experimental temperatures are deviations of about a factor of 2 observed. These remaining discrepancies can be easily explained by a slightly overpredicted temperature dependence. Unfortunately, the expected inversion of the temperature dependence could not be observed in the experiments. Obviously, at pressures below $p < 1$ bar, the rate constant minimum arise at temperatures $T < 700$ K. Combining the low-temperature data of Kappler and the high-temperature rate constants determined in this work, a rough estimate of $T \approx 500$ K can be made for $p = 133$ mbar, hence ≈150 K lower than calculated by Yang et al.

The switch from a negative to a positive temperature dependence can be explained by the competition of an association and an abstraction reaction mechanism. The dominating reaction channels of the potential energy surface as it has been explored by Yang et al.[18] are reproduced in Figure 8. Additional reaction channels leading to CNO + N_2O or CN + N_2O_2 do not play a role due to very high associated barriers.

Similar to the reaction NCN + NO, at low temperatures the reaction is a typical example of an association reaction forming the collisionally stabilized recombination product $NCNNO_2$. The sequential transition state lies energetically too high, (116 kJ/mol above the minimum, 34 kJ/mol above the entrance energy) such that the thermodynamically most stable products NCO and N_2O are not formed. At high temperatures, with a threshold energy of $E_0 = 41$ kJ/mol, a direct abstraction reaction channel becomes accessible. Here, an O atom is abstracted from NO_2 yielding the high-temperature reaction products NCNO and NO. According to Yang et al., even at high temperatures the contribution of the reaction channel forming NCO + N_2O remains negligible. Corresponding rate constants are predicted to be several orders of magnitude lower than for the NCNO + NO channel.

The positive temperature dependence of the overall reaction, which has been determined in this work, supports the proposed reaction mechanism. The measured Arrhenius activation energy of $E_a = 38.0$ kJ/mol is in close agreement with the calculated threshold energy of $E_0 = 41$ kJ/mol corresponding to the direct NCNO + NO abstraction channel.

IV. CONCLUSION

For the first time, high-temperature rate constants of the reactions NCN + NO → N_2O + CN (10) and NCN + NO_2 → NCNO + NO (11) have been measured. For reaction 10, rate constants are represented by the Arrhenius expression $k_{10}/(\mathrm{cm^3\,mol^{-1}s^{-1}}) = 1.9 \times 10^{12} \exp[-26.3(\mathrm{kJ/mol})/RT]$ in the temperature range 764 K < T < 1944 K. The experimentally accessible temperature range was limited by the decomposition rate of the NCN precursor NCN_3 at the lower bound and too small NCN absorption cross sections at high temperatures. Regarding reaction 11, the expression $k_{11}/(\mathrm{cm^3\,mol^{-1}s^{-1}}) = 4.7 \times 10^{12} \exp[-38.0(\mathrm{kJ/mol})/RT]$ accounts for the measured data points in the temperature range 691 K < T < 1659 K. Here, the temperature range was limited by the onset of the NO_2 decomposition and interfering secondary chemistry. In striking contrast to previous low temperature studies, at high temperatures no pressure but a pronounced positive temperature dependence has been determined. For reaction 10, $E_a = (26.3 \pm 1.6)$ kJ/mol and for reaction 11 $E_a = (38.0 \pm 3.8)$ kJ/mol. These values are in agreement with theoretical predictions and prove the postulated change of the overall reaction from a recombination to an abstraction-like pathway. Together with the low-temperature data taken from the literature, the position of the minimum of the overall reaction rate constant has been estimated to be around $T \approx 670$ K for reaction 10 and $T \approx 500$ K for reaction 11. Additionally, the influence of NO and NO_2 on the CIISC process, which transfers electronically excited ^{1}NCN to the ^{3}NCN ground state, has been investigated. With respect to CIISC probability, NO and NO_2 are 400 and 40 times more efficient collision partners than argon, respectively.

■ ASSOCIATED CONTENT

Supporting Information. Tables of the experimental data and conditions as well as temperature-dependent absorption cross sections of NO_2 can be found in the Supporting Information. This information is available free of charge via the Internet at http://pubs.acs.org.

■ AUTHOR INFORMATION

Corresponding Author
*Electronic address: friedrichs@phc.uni-kiel.de.

■ ACKNOWLEDGMENT

We would like to thank the German Science Foundation (FR 1529/4), the cluster of excellence "The Future Ocean" (DFG - EC 80), and Friedrich Temps for financial and scientific support. Thanks to Anna Busch, Claudia Kappler, Matthias Olzmann, and Oliver Welz (Karlsruher Institut für Technologie, KIT) for sharing data prior to publication.

■ REFERENCES

(1) Warnatz, J.; Maas, U.; Dibble, R. W. *Combustion*, 3rd ed. ; Springer: Berlin/Heidelberg, 2001.

(2) Harrison, R. M., Ed. *Principles of Environmental Chemistry*; RSC Publishing: Cambridge, 2007.

(3) Forster, P.; Ramaswamy, V.; Artaxo, P.; Berntsen, T.; Betts, R.; Fahey, D.; Haywood, J.; Lean, J.; Lowe, D.; Myhre, G.; Nganga, J.; Prinn, R.; Raga, G.; Schulz, M.; Dorland, R. V. *Climate Change 2007: The Physical Science Basis. Contribution of Working Group I to the Fourth Assessment Report of the Intergovernmental Panel on Climate Change*; Solomon, S., Qin, D., Manning, M., Chen, Z., Averyt, M. M. K., Tignor, M., Miller, H., Eds.; Cambridge University Press: Cambridge, United Kingdom, 2007.

(4) Glarborg, P.; Alzueta, M. U.; Dam-Johansen, K.; Miller, J. A. *Combust. Flame* **1986**, *65*, 177–202.
(5) Zeldovich, Y. B. *Acta Physicochim. USSR* **1946**, *21*, 577–628.
(6) Baulch, D. L.; Cobos, C. J.; Cox, A. M.; Frank, P.; Hayman, J.; Kerr, J. A.; Murrels, T.; Pilling, M. J.; Troe, J.; Walker, R. W.; Warnatz, J. *J. Phys. Chem. Ref. Data* **1994**, *23*, 847–1033.
(7) Wolfrum, J. *Chemieingenieurtechnik* **1972**, *44*, 656–659.
(8) Malte, P. C.; Pratt, D. T. *Proc. Combust. Inst.* **1974**, *15*, 1061–1070.
(9) Fenimore, C. P. *Proc. Combust. Inst.* **1971**, *13*, 373–380.
(10) Cui, Q.; Morokuma, K.; Bowman, J. M.; Klippenstein, S. J. *J. Chem. Phys.* **1999**, *110*, 9469–9482.
(11) Moskaleva, L. V.; Lin, M. C. *Proc. Combust. Inst.* **2000**, *28*, 2393–2401.
(12) Moskaleva, L. V.; Xia, W. S.; Lin, M. C. *Chem. Phys. Lett.* **2000**, *331*, 269–277.
(13) Smith, G. P. *Chem. Phys. Lett.* **2003**, *367*, 541–548.
(14) Sutton, J. A.; Williams, B. A.; Fleming, J. W. *Combust. Flame* **2008**, *153*, 465–478.
(15) Klein-Douwel, R. J. H.; Dam, N. J.; ter Meulen, J. J. *Opt. Lett.* **2008**, *33*, 2620–2622.
(16) Vasudevan, V.; Hanson, R. K.; Bowman, C. T.; Golden, D. M.; Davidson, D. F. *J. Phys. Chem. A* **2007**, *111*, 11818–11830.
(17) Huang, C.-L.; Tseng, S. Y.; Wang, T. Y.; Wang, N. S.; Xu, Z. F.; Lin, M. C. *J. Chem. Phys.* **2005**, *122*, 184321/1–9.
(18) Yang, T.-J.; Wang, N. S.; Lee, L. C.; Xu, Z. F.; Lin, M. C. *J. Phys. Chem. A* **2008**, *112*, 10185–10192.
(19) Chen, H.-T.; Ho, J.-J. *J. Phys. Chem. A* **2005**, *109*, 2564–2571.
(20) Wei, Z.-G.; Li, Q.-S.; Zhang, S.-W.; Sun, Y.-B.; Sun, C.-C. *J. Mol. Struc. - THEOCHEM* **2005**, *722*, 139–146.
(21) Zhu, R. S.; Lin, M. C. *Int. J. Chem. Kinet.* **2005**, *37*, 593–598.
(22) Zhu, R. S.; Lin, M. C. *J. Phys. Chem. A* **2007**, *111*, 6766–6771.
(23) Zhu, R. S.; Nguyen, M. T.; Lin, M. C. *J. Phys. Chem. A* **2009**, *113*, 298–304.
(24) Baren, R. E.; Hershberger, J. F. *J. Phys. Chem. A* **2002**, *106*, 11093–11097.
(25) Welz, O. Laserspektroskopische Untersuchungen und Molekularkinetische Modellierung der Kinetik von Radikalreaktionen in der Gasphase, Ph.D. Thesis, Universität Karlsruhe (TH), Universitätsverlag Karlsruhe, Karlsruhe, 2009, ISBN 978−3-86644−356−3.
(26) Kappler, C. Untersuchungen komplexbildender bimolekularer Reaktionen in der Gasphase mit laserspektroskopischen Methoden und statistischer Reaktionstheorie, Ph.D. Thesis, Karlsruher Institut für Technologie, KIT Scientific Publishing, Karlsruhe, 2010, ISBN 978−3-86644−567−3.
(27) Lamoureux, N.; Desgroux, P.; Bakali, A. E.; Pauwels, J. F. *Combust. Flame* **2010**, *157*, 1923–1941.
(28) El Bakali, A.; Pillier, L.; Desgroux, P.; Lefort, B.; Gasnot, L.; Pauwels, J. F.; da Costa, I. *Fuel* **2006**, *85*, 896–909.
(29) Gersen, S.; Mokhov, A. V.; Levinsky, H. B. *Combust. Flame* **2008**, *155*, 267–276.
(30) Konnov, A. A. *Combust. Flame* **2009**, *156*, 2093–2105.
(31) Sepman, A. V.; Mokhov, A. V.; Levinsky, H. B. *Int. J. Hydrogen Energy* **2011**, *36*, 4474–4481.
(32) Busch, A.; Olzmann, M. *Shock-Tube Study of the Thermal Decomposition of NCN*, Vienna, paper p810138, Proc. European Combust. Meeting, 2009.
(33) Busch, A. Stoßwellenuntersuchungen zum Zerfall stickstoffhaltiger Verbindungen mit spektroskopischen Methoden, Ph.D. Thesis, Karlsruher Institut für Technologie, KIT Scientific Publishing, Karlsruhe, 2010, ISBN 978−3-86644−586−4.
(34) Dammeier, J.; Friedrichs, G. *J. Phys. Chem. A* **2010**, *114*, 12963–12971.
(35) Dammeier, J.; Faßheber, N.; Friedrichs, G. *Phys. Chem. Chem. Phys.* DOI: 10.1039/c1cp22123j.
(36) Dammeier, J.; Colberg, M.; Friedrichs, G. *Phys. Chem. Chem. Phys.* **2007**, *9*, 4177–4188.
(37) Colberg, M.; Friedrichs, G. *J. Phys. Chem A* **2006**, *110*, 160–170.
(38) Klatt, M. Quantitative Untersuchung der Bildung und des Verbrauchs von H- und O-Atomen sowie OH-Radikalen in verschiedenen Elementarreaktionen bei hohen Temperaturen., Ph.D. Thesis, Universität Göttingen, 1991.
(39) Kee, R. J.; Ruply, F. M.; Miller, J. A. *Chemkin-II: A Fortran Chemical Kinetics Package for the Analysis of Gas Phase Chemical Kinetics*; Sandia report sand89-8009; Sandia National Laboratories: Livermore, CA, 1989.
(40) Smith, G. P.; Golden, D. M.; Frenklach, M.; Moriarty, N. W.; Eiteneer, B.; Goldenberg, M.; Bowman, C. T.; Hanson, R. K.; Song, S.; Jr., W. C. G.; Lissanski, V. V.; Qin, Z. GRI-MECH 3.0, http://www.me.berkeley.edu/gri_mech/.
(41) Konnov, A. A. Detailed reaction mechanisms for small hydrocarbon combustion, http://homepages.vub.ac.be/akonnov/science/mechanism/version0_5.html, 2007, release 0.5.
(42) Goos, E.; Burcat, A.; Ruscic, B. Ideal Gas Thermochemical Database with updates from Active Thermochemical Tables, ftp://ftp.technion.ac.il/pub/supported/aetdd/thermodynamics, 2010.
(43) Milligan, D. E.; Jacox, M. E.; Bass, A. M. *J. Chem. Phys.* **1965**, *43*, 3149–3160.
(44) Dammeier, J.; Oden, B.; Friedrichs, G. A consistent model for the thermal decomposition of NCN_3 and the singlet-triplet relaxation of NCN. *Int. J. Chem. Kinet.*, submitted for publication.
(45) Hack, W.; Wilms, A. *J. Phys. Chem.* **1989**, *93*, 3540–3546.
(46) Freed, K. F. *Adv. Chem. Phys.* **1981**, *47*, 291–336.
(47) Bley, U.; Temps, F. *J. Chem. Phys.* **1993**, *98*, 1058–1072.
(48) Slack, M. W. *J. Chem. Phys.* **1975**, *64*, 228–236.
(49) Delon, A.; Georges, R.; Kirmse, B.; Jost, R. *Faraday Discuss.* **1995**, *102*, 117–128.
(50) Bogumil, K.; Orphal, J.; Homann, T.; Voigt, S.; Spietz, P.; Fleischmann, O.; Vogel, A.; Hartmann, M.; Kromminga, H.; Bovensmann, H.; Frerick, J.; Burrows, J. *J. Photochem. Photobiol. A* **2003**, *157*, 167–184.
(51) Röhrig, M.; Petersen, E. L.; Davidson, D. F.; Hanson, R. K. *Int. J. Chem. Kinet.* **1996**, *28*, 599–608.
(52) Atkinson, R.; Baulch, D. L.; Cox, R. A.; Hampson, R. F.; Kerr, J. A.; Troe, J. *J. Phys. Chem. Ref. Data* **1989**, *18*, 881–1108.